## PAPER

Cite this: *Nanoscale*, 2025, **17**, 11624

# Cobaltabis(dicarbollide) [*o*-COSAN]⁻ loaded apoferritin: an innovative high-capacity boron delivery system to target tumour cells for BNCT applications†

D. Alberti, [ID] [a] J. N. Piña Marcos,[a] S. Rakhshan,[a] N. Protti,[b,c] S. Altieri,[b,c] M. Nuez-Martínez,[d] F. Teixidor, [ID] [d] C. Viñas [ID] [d] and S. Geninatti Crich [ID] *[a]

This study describes an innovative apoferritin-based nanohybrid, Apo:[*o*-COSAN]⁻, as a high-capacity boron delivery system for potential application in boron neutron capture therapy (BNCT). The nanohybrid is characterized by a high boron content, stability, and the promotion of biological interactions of cobalta-bis(dicarbollide) ([*o*-COSAN]⁻), encapsulated within the apoferritin protein cavity through an acid-induced dissociation and reassembly process. The Apo:[*o*-COSAN]⁻ nanohybrid demonstrated enhanced boron uptake in MCF7 breast cancer and AB22 mesothelioma cell lines, with superior stability and biocompatibility under physiological conditions. Notably, AB22 cells treated with Apo:[*o*-COSAN]⁻ showed significant cytotoxic effects following neutron irradiation, highlighting the potential of this system in BNCT. These findings underscore the versatility of apoferritin as a multifunctional nanocarrier for targeted cancer therapy, combining high boron payloads with selective tumour cell uptake.

## Introduction

The efficacy of a pharmaceutical agent is significantly influenced by its capacity to accumulate at the target site in therapeutic concentrations. However, various challenges, such as rapid renal clearance, drug degradation, and non-specific accumulation in off-target tissues, can hinder this process. To overcome these obstacles and enhance drug delivery, there is a growing demand for advanced drug delivery technologies that promote targeted accumulation and sustained release, thereby improving therapeutic outcomes and reducing side effects. In this context, naturally occurring protein cages have emerged over the past two decades as promising tools for a range of pharmaceutical applications, particularly in the field of drug delivery.[1–3] Protein cages are ideal platforms as they are self-assembled into uniform cages, compatible, biodegradable, bioavailable, abundant renewable sources and, naturally tar-

geted to specific receptors. Ferritin is a 12 nm spherical protein made up of 24 light (L) or heavy (H) chain peptide sub-units arranged in a cage architecture with an 8 nm interior cavity that can hold up to 4500 iron atoms.[4,5] After the iron is taken out, the spherical hollow core of ferritin, named apoferritin,[6,7] can be used to load different kinds of cargo into its internal cavity or to bind to its surface, through hydrogen bonding or electrostatic interactions.[8–10] The cargoes can include biologically active substances, complexes, and other metal ions.[11–15] This has potential applications in a wide range of biomedical fields particularly in oncological research, as the protein is internalized by cells through selective receptors overexpressed on tumour cells.[16] Although many examples of the successful delivery of drugs or imaging probes by apoferritin have been reported in the literature, to our knowledge, this is the first time it has been proposed for the delivery of boron-containing molecules for boron neutron capture therapy (BNCT). BNCT is a radiation-based therapy that is emerging as a promising tool in the treatment of cancer.[17,18] In brief, the therapy involves selectively concentrating boron compounds in tumour cells and then exposing the tumour cells to epithermal neutron radiation. BNCT describes the nuclear reaction that occurs when a stable isotope, boron-10 ($^{10}$B), is irradiated with low-energy thermal neutrons. This reaction produces recoiling lithium-7 nuclei and α particles or helium-4. For BNCT to be effective, a significant number of $^{10}$B atoms must be localised on or within neoplastic cells.[19] In addition, the $^{10}$B atoms must

*[a]Department of Molecular Biotechnology and Health Sciences, University of Torino, Via Nizza, 52, 10126 Turin, Italy. E-mail: simonetta.geninatti@unito.it*
*[b]Department of Physics, University of Pavia, Via Agostino Bassi 6, 27100 Pavia, Italy*
*[c]Nuclear Physics National Institute (INFN), Unit of Pavia, Via Agostino Bassi 6, 27100 Pavia, Italy*
*[d]Institut de Ciència de Materials de Barcelona (ICMAB-CSIC), Campus UAB, 08193 Bellaterra, Spain*
†Electronic supplementary information (ESI) available. See DOI: https://doi.org/10.1039/d5nr00362h

absorb a sufficient amount of thermal neutrons to sustain a lethal $^{10}$B $(n, \alpha)$ lithium-7 reaction. The ability of BNCT to deposit a massive dose gradient between normal and tumour cells is its most unique feature.[20] Developing boron delivery systems that are highly targeted, effective, non-toxic, and biodegradable is a major challenge towards realizing the great potential of BNCT.[21–27] In this study, we propose to use L-chain-rich horse spleen apoferritin (abbreviated as Apo) to selectively deliver $^{10}$B to MCF7 breast cancer cells and AB22 mesothelioma cells by using cobaltabis(dicarbollide) $([3,3'-Co(1,2-C_2B_9H_{11})_2]^-$, abbreviated as $[o\text{-COSAN}]^-$) an anionic boron cluster containing 18 boron atoms.[28–31] Apo is taken up by cells through the scavenger receptor class A member 5 (SCARA5).[32,33] This receptor is believed to play an important role in the development and progression of several tumour types, displaying different expression pattern when compared to normal tissues.[34,35] Breast cancer has been already studied by our group through the exploitation of Apo as a helpful transporter of therapeutics and imaging probes for MRI-guided treatment of MCF7 breast cancer cells that exhibit ferritin uptake.[36] Mesothelioma represents a rare yet highly aggressive form of cancer that primarily affects the pleural lining of the lungs. Its pathogenesis is strongly linked to occupational and environmental exposure to asbestos, a known carcinogen.[37] The disease typically manifests several decades after initial exposure, leading to significant morbidity and mortality. In recent years, there was a growing interest in exploring innovative treatment strategies for mesothelioma, including BNCT.[38–43] Such advancements in treatment strategies are crucial given the poor prognosis associated with mesothelioma, underscoring the need for continued research into effective interventions for this challenging malignancy. The use of $[o\text{-COSAN}]^-$ has several advantages:[44] 1) high boron content (18 atoms/molecule),[45,46] (2) membrane crossing ability,[47] and (3) DNA binding ability.[48] Moreover, Na[$o$-COSAN] is remarkably stable,[49] water-soluble,[50] and interact with various biological molecules,[51] is cytostatic, not cytotoxic.[52] The properties of $[o\text{-COSAN}]^-$ as specific and potent inhibitors of HIV protease was first reported in 2005.[51] Later, the nature of $[o\text{-COSAN}]^-$ interactions with proteins *via* dihydrogen bonds was experimentally demonstrated,[53] and the amino acids involved in the strongest interactions (lysine, arginine and histidine) were identified and described.[54,55] In this article, we present the preparation of the Apo:$[o\text{-COSAN}]^-$ nanohybrid, achieved through the encapsulation of $[o\text{-COSAN}]^-$ anionic clusters within the apoferritin protein cavity, designed as a targeted delivery system for tumour cells in boron neutron capture therapy (BNCT) applications.

# Results and discussion

### Strategy for encapsulation of $[o\text{-COSAN}]^-$ molecules in apoferritin cavity.

A remarkably high cargo loading capacity of Apo was achieved by exploiting an encapsulation strategy, which disaggregates its nanostructure in an acidic environment (pH = 2) and subsequently reassembles under physiological pH conditions (pH = 7.4) (Fig. 1). The goal of employing this method was to efficiently incorporate $[o\text{-COSAN}]^-$ into the Apo cavity, concentrating a large number of boron-containing $[o\text{-COSAN}]^-$ molecules required for an effective BNCT treatment within the internal protein cavity.

Apo loading capability of $[o\text{-COSAN}]^-$ molecules was investigated by incubating Apo with increasing concentrations of $[o\text{-COSAN}]^-$, spanning molar ratios from 9 to 600 $[o\text{-COSAN}]^-$ molecules per apoferritin. To evaluate the efficiency of the encapsulation strategy, $[o\text{-COSAN}]^-$ was incubated with the protein in both its dissociated (at pH = 2) (Apo:$[o\text{-COSAN}]^-$) and its non-dissociated form (Apo:$[o\text{-COSAN}]^-$ control). Then, the resultant mixture was dialyzed (4 °C) against 0.15 M NaCl/ HEPES buffer (pH = 7.4) using a membrane with a molecular weight cutoff (MWCO) of 14 kDa to remove any remaining unbound $[o\text{-COSAN}]^-$ molecules. The assessment of the amount of $[o\text{-COSAN}]^-$ encapsulated into the Apo was carried out by measuring the B concentration by ICP-MS and the mg of the protein remained after the purification process (see details below).

As shown in Fig. 2, the acidic dissociation method was able to entrap a higher number of $[o\text{-COSAN}]^-$ clusters in the Apo cavity compared to the simple incubation with the non-dissociated Apo where the $[o\text{-COSAN}]^-$ clusters interact non-specifically with the Apo outer surface.

### Characterization of apoferritin nanohybrids loaded with increasing concentrations of $[o\text{-COSAN}]^-$ molecules.

Different Apo:$[o\text{-COSAN}]^-$ nanohybrids were then analysed by IR spectrometry. In fact, the characteristic B–H band of borane clusters in Na[$o$-COSAN]$^-$ solid appears in a unique region of the IR spectrum, around 2500 cm$^{-1}$, where no other bonds are present (Fig. S1A†). The $\nu$(B–H) peaks around 2500 cm$^{-1}$ were confirmed in the Apo:$[o\text{-COSAN}]^-$ nanohybrid with a final
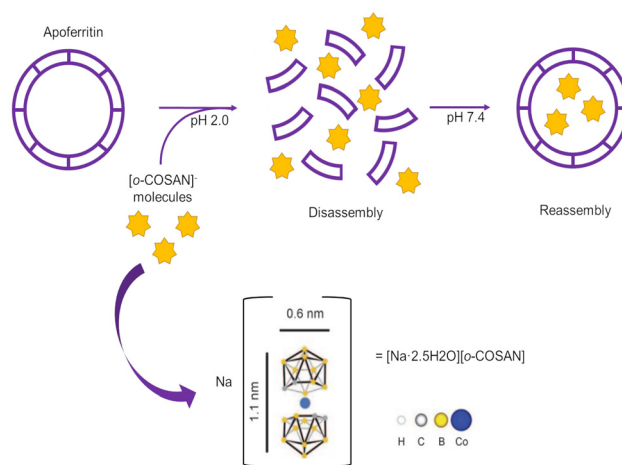


**Fig. 1** Schematic representation of $[o\text{-COSAN}]^-$ molecules encapsulation strategy in the apoferritin cavity using the pH changing method.
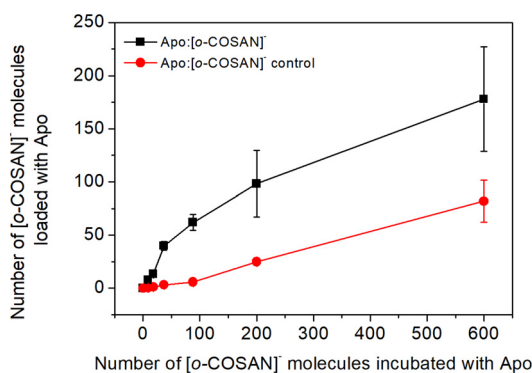
**Fig. 2** Apoferritin loading capability of $[o\text{-COSAN}]^-$ molecules performed with disassembly and reassembly of Apo at pH = 2 (Apo:$[o\text{-COSAN}]^-$) (black squares) or without the acid pH dissociation of the protein shell (Apo:$[o\text{-COSAN}]^-$ control) (red circles).

protein/$[o\text{-COSAN}]^-$ ratio of 1 : 71, prepared using the dissociation method at acid pH. The IR spectra indicate that the acidic Apo dissociation and subsequent reassembling method incorporates a greater number of $[o\text{-COSAN}]^-$ clusters compared to the simple incubation method using non-dissociated Apo (with a protein/$[o\text{-COSAN}]^-$ ratio of only 1 : 6) (Fig. S1B†). As expected, the sensitivity of this technique does not allow the detection of the B–H peak in the Apo:$[o\text{-COSAN}]^-$ at ratio 1 : 14 and Apo:$[o\text{-COSAN}]^-$ control at ratio 1 : 2 probably due to the low boron concentration in the sample (Fig. S1C†).

Apo:$[o\text{-COSAN}]^-$ nanohybrids, loaded with increasing concentrations of $[o\text{-COSAN}]^-$ (prepared *via* the dissociation method at acidic pH = 2), were analysed using fast protein liquid chromatography (FPLC). Chromatograms acquired at 215 nm were compared to native Apo (Fig. 3A). The results indicate that Apo loaded with ≤8 $[o\text{-COSAN}]^-$ clusters exhibit the same retention volume as native Apo ($V_r$ = 14.4 mL). However, a second peak at $V_r$ = 17.4 mL, corresponding to an adduct with a smaller hydrodynamic radius, contributing ≤25% to the total area ($V_r$ = 14.4 and 17.4 mL), was observed. This second peak at

$V_r$ = 17.4 mL increases to 35% of the total area when Apo was loaded with 14 $[o\text{-COSAN}]^-$ molecules. On the contrary, Apo samples loaded with >14 were no longer able to reassociate correctly and present either the two peaks at $V_r$ = 14.4 and 17.4 mL with similar area or just a single peak at $V_r$ = 17.4 mL corresponding to a species with lower molecular weight. This agrees with DLS measurements. As shown in Fig. 3B, increasing the ratio of $[o\text{-COSAN}]^-$ molecules to Apoferritin resulted in a reduction in the diameter of the refolded protein. The size decreased from approximately 14 nm (the diameter of both native Apo and Apo loaded with ≤8 $[o\text{-COSAN}]^-$ molecules) to approximately 9.4 ± 1.1 nm when loaded with >14 $[o\text{-COSAN}]^-$ molecules. To ensure the preservation of correct protein architecture, only Apo:$[o\text{-COSAN}]^-$ nanohybrids containing ≤8 $[o\text{-COSAN}]^-$ molecules were selected for further investigation. Various preparations ($n$ = 8) of Apo loaded with 6.1 ± 1.7 $[o\text{-COSAN}]^-$ molecules were obtained by incubating Apo:$[o\text{-COSAN}]^-$ at ratio 1 : 9. These preparations were used to generate the results presented in the following sections of this paper.

### Stability of Apo:$[o\text{-COSAN}]^-$ nanohybrids.

The stability of the Apo:$[o\text{-COSAN}]^-$ was evaluated by dialyzing the samples in a 0.15 M NaCl/HEPES buffer (pH = 7.4) (MWCO = 14 kDa) at 37 °C under stirring for 24 hours. The release of $[o\text{-COSAN}]^-$, quantified through boron measurement using the ICP-MS technique, reached a maximum of 20% after 24 hours, demonstrating the nanohybrid overall stability under physiological conditions (Fig. 4).

### Uptake of Apo:$[o\text{-COSAN}]^-$ nanohybrids in human breast MCF7 and murine mesothelioma AB22 cell lines.

Uptake studies were carried out to explore the ability of Apo:$[o\text{-COSAN}]^-$ to specifically deliver boron atoms to MCF7 (human breast cancer) and AB22 (murine mesothelioma) cells. Fig. 5A shows that Apo:$[o\text{-COSAN}]^-$ incubated for 6 h in the presence of MCF7 cells exhibited significantly higher boron internalization compared to free $[o\text{-COSAN}]^-$ in the range 1–13 μM and
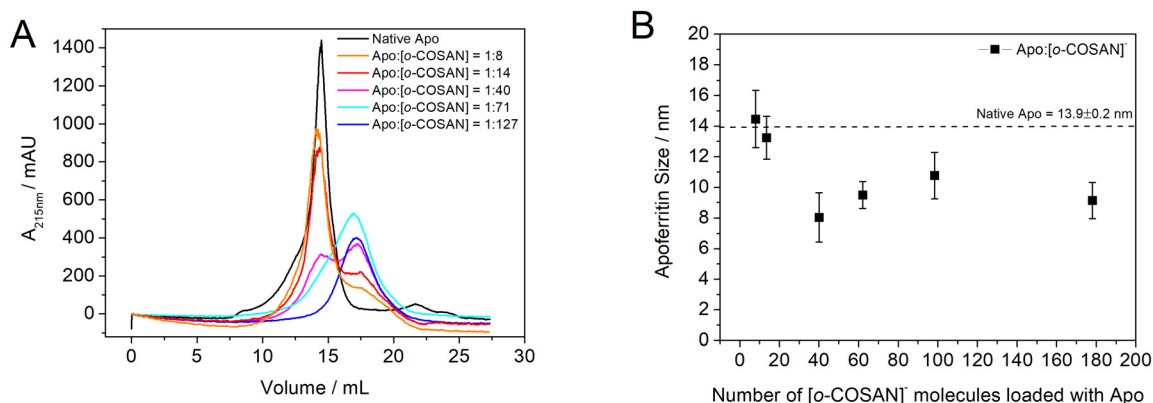


**Fig. 3** (A) FPLC chromatography showing retention volumes ($V_r$) of native apoferritin or Apo:$[o\text{-COSAN}]^-$ samples loaded with increasing $[o\text{-COSAN}]^-$ concentrations, acquired at 215 nm (protein signal) and (B) DLS characterization of Apo samples loaded with increasing concentrations of $[o\text{-COSAN}]^-$.
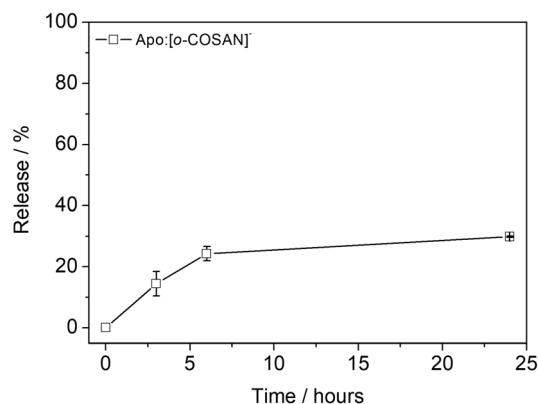
**Fig. 4** Stability of Apo loaded [$o$-COSAN]$^-$ molecules (Apo:[$o$-COSAN]$^-$ nanohybrid) dialyzed in 40 mL of 0.15M NaCl/HEPES buffer (pH 7.4) at 37 °C, under stirring, for 24 h.

its trend clearly indicates a saturation behaviour. Up to 16 hours of incubation (Fig. 5B), the amount of internalized boron remained unchanged, indicating no additional benefit from extending the incubation time. Moreover, the prolonged incubation led to an increased nonspecific uptake of free [$o$-COSAN]$^-$ when incubated alone. The [$o$-COSAN]$^-$ used in this study, contains only natural abundant boron; thus, the maximum amount of $^{10}$B internalized, upon incubation with 13 μM Apo:[$o$-COSAN]$^-$ concentration, calculated as 19.9% of the total boron was of *ca.* 0.7 μg per g of tissue. The conversion cell number to g of tissue was performed assuming that in the case of epithelial tumours (with a diameter ranging 15–20 μm), a density of *ca.* $10^8$ cells for cm$^3$ is a reasonable number for these tumour tissues.[56] Given the low boron concentration (ppm) measured in these cells, neutron irradiation was not pursued.

Although a similar internalization of Apo:[$o$-COSAN]$^-$ and free [$o$-COSAN]$^-$ was observed in the 10–50 μM concentration range for AB22 mesothelioma cells (not significant (ns) $p >$ 0.05. See details in Table S1†), these cells exhibited a signifi-

cantly higher uptake capability compared to MCF7 cells (Fig. 6A). Interestingly, the maximum amount of $^{10}$B internalized in AB22 cells upon incubation with 50 μM [$o$-COSAN]$^-$ was 4 μg per g of tissue, a concentration sufficient to proceed with neutron irradiation. Additionally, cells incubated with Apo:[$o$-COSAN]$^-$ displayed a slightly reduced proliferation rate, likely due to the cytostatic effect of [$o$-COSAN]$^-$, as previously reported in the literature.[52] Interestingly, when delivered *via* the apoferritin vector, [$o$-COSAN]$^-$ demonstrated a 20% increase in toxicity (Fig. 6B). Similar results were obtained with MCF7 cells as reported in ESI (Fig. S2†).

The specific mediation of Apo:[$o$-COSAN]$^-$ nanohybrids uptake was performed by competition experiments carried out with polyinosinic acid, a specific SCARA receptors inhibitor,[57] preincubated 30 min before the addition of Apo:[$o$-COSAN]$^-$ nanohybrids. The amount of boron internalized by cells after incubation with 20 μM Apo:[$o$-COSAN]$^-$ was reduced by the presence of polyinosinic acid in both MCF7 and AB22, thus confirming that SCARA5 mediates L-ferritin uptake in both cell lines (see details in Fig. S3†).

### SCARA5 detection

An immunofluorescence assay was performed to evaluate whether the differences in Apo:[$o$-COSAN]$^-$ uptake observed in MCF7 and AB22 cells were due to variations in SCARA5 receptor expression.

MCF7 and AB22 cells were seeded in μ-Slide 8 well ibidi and left in a cell incubator at 37 °C, 5% CO$_2$. 48 h later, the cells were fixed, stained for SCARA5 expression and examined using confocal microscopy. As shown in Fig. 7, both cell lines expressed SCARA5, but accordingly with uptake results, MCF7 showed a lower expression level with respect to AB22. Quantification of SCARA5 expression by ImageJ software showed that the mean fluorescence intensity values of AB22 were almost doubled in comparison to MCF7 (see details in Fig. S4†). Through the UALCAN web interface,[58,59] we successfully examined the gene expression data from the cancer genome atlas (TCGA), which indicated that SCARA5 expression
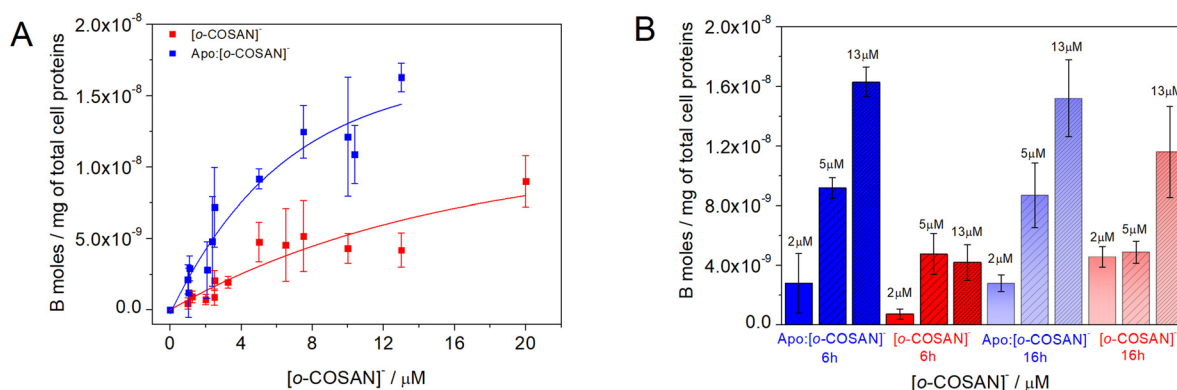


**Fig. 5** (A) Uptake study performed on MCF7 cells incubated with increasing concentration of Apo:[$o$-COSAN]$^-$ or free [$o$-COSAN]$^-$ molecules for 6 h at 37 °C, 5% CO$_2$. (B) A comparison of boron uptake by MCF7 cells incubated with either Apo:[$o$-COSAN]$^-$ or free [$o$-COSAN]$^-$ for 6 hours and 16 hours at 37 °C under 5% CO$_2$ conditions.
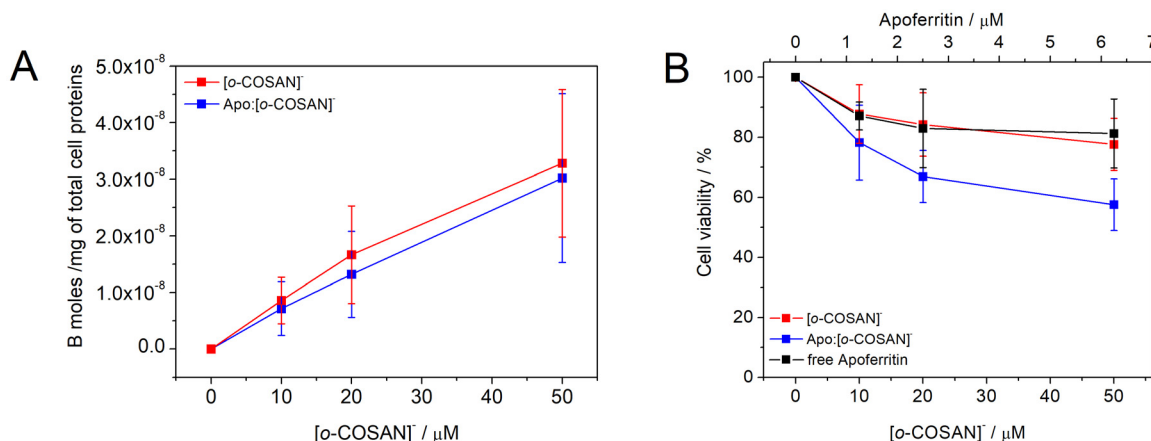
**Fig. 6** Uptake study performed on AB22 mesothelioma cells incubated with increasing concentrations of Apo:[o-COSAN]⁻ nanohybrid (in blue) or free [o-COSAN]⁻ molecules (in red) for 16 h at 37 °C, 5% CO₂. (A) Boron concentration expressed as moles of boron per mg of cell proteins. (B) Percentage of viable cells measured by Bradford assay 16 h after incubation of AB22 cells with increasing concentrations of Apo alone (in black), Apo:[o-COSAN]⁻ nanohybrid or free [o-COSAN]⁻ molecules.
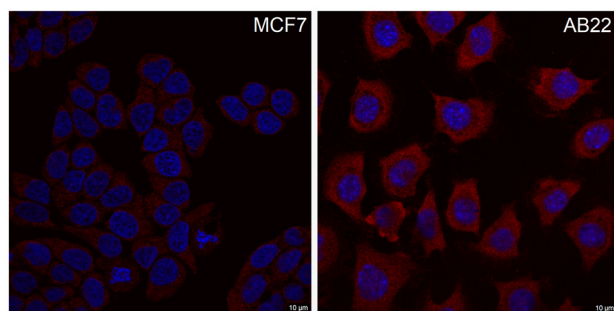


**Fig. 7** SCARA5 staining of MCF7 and AB22 cells plated on μ-Slide 8 well ibidi. Cell nuclei were counterstained with DAPI. Images of magnification 63× were acquired with Leica STELLARIS 8 confocal microscope.

(in terms of transcripts per million) is about 2.5 times lower in metastatic breast cancer with respect mesothelioma thus confirming the results obtained with immunofluorescence assay.

### *In vitro* BNCT treatment on AB22 mesothelioma cells

Based on the uptake results, AB22 cells were selected for BNCT applications, suggesting the potential for a targeted therapeutic approach to combat this aggressive disease. Accordingly, AB22 cells preincubated with either Apo:[o-COSAN]⁻ or free [o-COSAN]⁻ at a concentration of 50 μM [o-COSAN]⁻ for 16 hours at 37 °C under 5% CO₂ were exposed to thermal neutron irradiation (15 minutes at 30 kW reactor power) at the TRIGA II reactor at the University of Pavia. The long-term cytotoxic effects were subsequently assessed using a clonogenic assay.

24 hours post-irradiation, the number of surviving viable cells was assessed using the trypan blue exclusion assay. The study included six experimental groups: (1) untreated irradiated cells (CTRL IRR), (2) cells treated with [o-COSAN]⁻ and irradiated ([o-COSAN]⁻ IRR), and (3) cells treated with Apo:[o-COSAN]⁻ and irradiated (Apo:[o-COSAN]⁻ IRR), all of which

were exposed to thermal neutrons. The results (Fig. 8A) were compared to their corresponding non-irradiated groups, designated as (4) untreated cells (CTRL), (5) [o-COSAN]⁻ treated cells ([o-COSAN]⁻), and (6) Apo:[o-COSAN]⁻ treated cells (Apo:[o-COSAN]⁻).

Fig. 8A demonstrates that in both experimental groups treated with Apo:[o-COSAN]-, the number of surviving cells was significantly reduced by approximately 60% compared to the untreated controls, with no significant difference observed between the irradiated and non-irradiated groups. Notably, the clonogenic assay (Fig. 8B and Fig. S5†), performed 10 days post-irradiation on AB22 cells, revealed that only the cells subjected to BNCT treatment exhibited a markedly reduced colony-forming ability. This effect was particularly pronounced in the Apo:[o-COSAN]⁻ IRR group, which showed a 50% reduction in colony formation compared to the IRR CTRL group and an 80% reduction compared to the non-IRR CTRL group. In contrast, the negligible toxic effect observed following irradiation in the presence of [o-COSAN]⁻ alone underscores the more efficient intracellular localization of ¹⁰B achieved through delivery *via* apoferritin.

## Experimental

### General

Horse Speen Apoferritin and all other chemicals were purchased from Merck Life Science S.r.l., 20149 Milano (Italy). The sodium salt of cobaltabis(dicarbollide) Na[o-COSAN] was synthesized from Cs[o-COSAN][60] by using cationic exchanging resin as reported at the literature.[61]

### [o-COSAN]⁻ loading into apoferritin

The method for trapping small molecules inside the Apoferritin cavity was previously reported.[62] Briefly, in order to load [o-COSAN]⁻ molecules into the iron-free horse spleen apoferritin
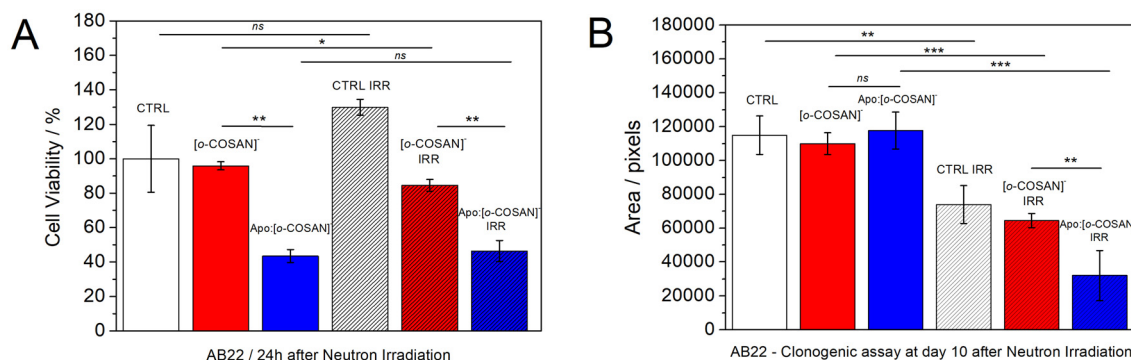
**Fig. 8** (A) Percentage of viable AB22 mesothelioma cells 24 h after neutron irradiation measured by trypan blue exclusion test. Control non treated and non-irradiated cells were set to 100% cell viability. (B) Clonogenic assay performed 10 days after neutron irradiation. Statistical analysis was performed by using student $t$-test: not significant (ns) $p > 0.05$, $*p \leq 0.05$, $**p \leq 0.01$ $***p \leq 0.001$ (see details in Table S2†).

cavity, the pH of a stirring protein solution (0.0585 μmol) was lowered to pH = 2 using 1 M HCl and maintained at this level for 15 minutes. Afterwards, varying volumes (5.7–380 μL) of a [$o$-COSAN]⁻ solution in water (92 mM) were added to achieve different Apoferritin/[$o$-COSAN]⁻ molar ratios (final volume, $V_f$ = 4 mL), ranging from 1:9 to 1:600. NaOH 1 M was used to raise the pH to 7.4. After being stirred for two hours at room temperature, the resultant mixture was dialyzed (4 °C) against 0.15 M NaCl/HEPES buffer (pH = 7.4) using a membrane with a molecular weight cutoff (MWCO) of 14 kDa to remove any remaining unbound [$o$-COSAN]- molecules. Finally, the Apo:[$o$-COSAN]⁻ nanohybrid solutions were centrifuged (3000 rpm, 5 min) to remove any further impurities and for uptake studies they were concentrated by Vivaspin centrifugal concentrators (MWCO = 50 kDa). To evaluate the efficiency of the encapsulation strategy, [$o$-COSAN]⁻ was incubated with the protein also in its non-dissociated form (Apo:[$o$-COSAN]⁻ control) following the procedure reported above to reach the different Apoferritin/[$o$-COSAN]⁻ molar ratios ranging from 1:9 to 1:600. The protein and [$o$-COSAN]⁻ concentrations were then measured by Bradford assay and by ICP-MS technique with boron analysis employed for [$o$-COSAN]⁻ quantification (see details below). The Malvern Zetasizer 3000HS (Malvern, UK) dynamic light scattering (DLS) system was utilized to determine the hydrated mean diameter of the Apo:[$o$-COSAN]⁻ nanohybrid.

### ATR-FTIR spectroscopy

Apo:[$o$-COSAN]⁻ nanohybrids with a protein/[$o$-COSAN]⁻ ratio of 1:71 (obtained after incubation at 1:88 molar ratio) and 1:14 (obtained after incubation at 1:18 molar ratio) and their respective Apo:[$o$-COSAN]⁻ controls at ratios 1:6 and 1:2, were analysed. ATR-FTIR experiments were performed on a JASCO 4700 spectrophotometer, 400–4000 cm⁻¹ (64 scans). Baseline, smoothing, and normalization (using 2920 cm⁻¹ peak) were performed using Jasco Spectra Manager software.

### Chromatography

The fast protein liquid chromatography (FPLC) characterization of the different Apo:[$o$-COSAN]⁻ nanohybrid preparations

was carried out on an Amersham Akta Purifier chromatographic system equipped with UV-Vis detector (set at 215 nm) and an Amersham Superose 6 size-exclusion column (10/300 GL, G.E. Healthcare). The experimental workup was carried out in an isocratic condition at 0.5 mL min⁻¹, using an aqueous mobile phase containing 0.15 M NaCl/HEPES buffer (pH = 7.4). The area under the peaks was calculated by Origin 8.5 software.

### Stability

Based on the results obtained in the previous characterization experiments, the stability and the next studies has been performed using the more promising Apo:[$o$-COSAN]⁻ nanohybrid obtained by incubating Apo:[$o$-COSAN] at ratio 1:9. Various preparations ($n = 8$) of Apo loaded with 6.1 ± 1.7 [$o$-COSAN]⁻ molecules were obtained to generate the results presented in the following sections of this paper.

To evaluate the stability, 2 mL of Apo:[$o$-COSAN]⁻ nanohybrid preparations, were dialyzed in 40 mL of 0.15 M NaCl/HEPES buffer at 37 °C for 24 hours (MWCO = 14 kDa). At various time intervals, aliquots of Apo:[$o$-COSAN]⁻ solutions were taken to measure protein and boron concentrations. The 40 mL NaCl/HEPES buffer was refreshed at each drawing. The amounts of boron were measured by ICP-MS. The percentage of boron released was calculated with eqn (1):

$$\%\text{Release} = \left( \frac{[B(t_0) - B(t_1)]}{B(t_0)} \right) \times 100 \qquad (1)$$

for which $B(t_1)$ is the amount of $B$ measured by ICP-MS inside the dialysis membrane at the various time intervals ($t = 0, 3, 6, 24$ h), and $B(t_0)$ is the amount of $B$ at the starting point ($t = 0$) of the stability test.

### Inductively coupled plasma mass spectrometry (ICP-MS)

By using inductively coupled plasma mass spectrometry (ICP-MS) (Element-2; Thermo-Finnigan, Rodano (MI), Italy), the boron content of [$o$-COSAN]⁻, Apo:[$o$-COSAN]⁻, Apo:[$o$-COSAN]⁻ control preparations and cell samples after [$o$-COSAN]⁻ and Apo:[$o$-COSAN]⁻ uptake was determined. A high-

performance microwave digestion system (ETHOS UP Milestone, Bergamo, Italy) was used to process the samples for 6 minutes at 150 °C, in a final volume of 0.4 mL after the addition of 70% concentrated $HNO_3$ to the samples (1 : 1). During sample runs, the naturally occurring abundant boron-standard solution was analysed to look for differences in the systematic bias. Four boron absorption standard solutions (Sigma-Aldrich) in the 0.1–0.004 µg mL$^{-1}$ range were used to generate the calibration curve.

### Cell lines

From the American Type Culture Collection (ATCC, USA), human MCF7 breast cancer cell line was acquired. MCF7 cells were cultivated in EMEM (Lonza) with 10% (v/v) Fetal Bovine Serum (FBS), 2 mM glutamine, 100 U mL$^{-1}$ penicillin, 100 U mL$^{-1}$ streptomycin, 1 mM sodium pyruvate, non-essential amino acids, and 10 µg mL$^{-1}$ human insulin (Sigma). AB22 murine mesothelioma cell line was purchased from Sigma Aldrich and was cultured in RPMI 1640 media supplemented with 25 mM HEPES (Lonza), 10% (v/v) Fetal Bovine Serum (FBS), 2 mM of L-glutamine (Lonza), 100 U mL$^{-1}$ penicillin and 100 U mL$^{-1}$ streptomycin (Lonza). MCF7 and AB22 cell lines were maintained at 37 °C in a 5% $CO_2$ incubator.

### Cell uptake

For *in vitro* uptake experiments, $7 \times 10^5$ MCF7 cells were seeded in T25 flasks. After 48 h and 24 h at 37 °C, 5% $CO_2$ in a cell incubator, the cells were incubated for 6 h and 16 h, respectively, with increasing concentrations of free [o-COSAN]$^-$ or Apo:[o-COSAN]$^-$ nanohybrids. Conversely, $4.75 \times 10^5$ AB22 cells were seeded in T25 flasks. After 24 h at 37 °C, 5% $CO_2$ in a cell incubator, the cells were incubated for 16 h with increasing concentrations of free [o-COSAN]$^-$ or Apo:[o-COSAN]$^-$ nanohybrids. After the incubation, MCF7 and AB22 cells were washed three times with 3 mL of ice-cold phosphate-buffered saline (PBS) and detached using a solution of 0.05% trypsin and 0.02% EDTA. Then, all cell samples were transferred in Falcon tubes, re-suspended in 200 µL of PBS and sonicated at 30% power in ice for 30 s. Moreover, the amount of protein of each cell sample was measured by Bradford assay (BioRad) using bovine serum albumin (BSA) as a standard. Finally, the boron content taken-up by each cell sample was evaluated by ICP-MS technique and normalised to its total protein content. From the mg of cell proteins measured by Bradford assay the cell number of each cell sample was obtained, using the calibration curve: [(mg protein)/(number of cells)]. From this calibration curve, 1 mg of MCF7 proteins correspond to 4.8 million of cells and 1 mg of AB22 proteins correspond to 1.65 million of cells. Finally, starting from ICP-MS data, it was possible to calculate µg g$^{-1}$ of boron by assuming a density of about $10^8$ cells per cm$^3$ in the case of epithelial tumours (with a diameter ranging 15–20 µm). Furthermore, the amount of protein of each cell sample determined by Bradford assay was used to indirectly calculate the percentage of viable cells after internalization with free [o-COSAN]$^-$ or Apo:[o-COSAN]$^-$ nano-

hybrids with respect to untreated control cell samples set to 100% viability.

### Competition

For *in vitro* competition experiments, $7 \times 10^5$ MCF7 and $4.75 \times 10^5$ AB22 cells were seeded in T25 flasks. After 48 h and 24 h, respectively, at 37 °C, 5% $CO_2$ in a cell incubator, MCF7 cells were incubated for 6 h and AB22 for 16 h with 20 µM Apo:[o-COSAN]$^-$ in the absence or in the presence of 0.1 mg mL$^{-1}$ of polyinosinic acid (Sigma) preincubated 30 min before adding Apo:[o-COSAN]$^-$. After the incubation, MCF7 and AB22 cells were washed three times with 3 mL of ice-cold PBS and detached using a solution of 0.05% trypsin and 0.02% EDTA. Then, all cell samples were transferred in Falcon tubes, re-suspended in 200 µL of PBS and sonicated at 30% power in ice for 30 s. Moreover, the amount of protein of each cell sample was measured by Bradford assay (BioRad) using bovine serum albumin as a standard. Finally, the boron content taken-up by each cell sample was evaluated by ICP-MS technique and normalised to its total protein content.

### Immunofluorescence

For immunofluorescence experiment, $3 \times 10^4$ MCF7 and $1 \times 10^4$ AB22 cells were seeded in a µ-Slide 8 well ibidi (code 80826). After 48 h at 37 °C, 5% $CO_2$ in a cell incubator, the cell culture medium was removed and the cells were rinse 2 times using 200 µL of PBS. The cells were fixed using 200 µL of 4% paraformaldehyde (pH 7.4) for 10 minutes at 37 °C. Paraformaldehyde solution was then removed and the cells were washed 3 times with 200 µL of PBS. The cells were incubated at room temperature for 15 min with 200 µL of 0.1% Triton X-100 (Sigma) in PBS. Triton-X-100 was removed, and the cells were washed two times with 200 µL of PBS. 200 µL of 10% BSA (Sigma) in PBS was added to the cells that were incubated at room temperature for 20 minutes. Then, anti-SCARA5 primary antibody (Santa Cruz, sc-98123) diluted 1 : 25 in 200 µL of 1% BSA was added to the cells and incubated for 3 hours at room temperature. After the incubation, anti-SCARA5 primary antibody was removed and the cells were washed three times with 200 µL of PBS. Subsequently, Texas Red-conjugated goat anti-rabbit secondary antibody (Invitrogen, T2767) diluted 1 : 500 in 200 µL of 1% BSA was added to the cells and incubated for 60 minutes at room temperature protected from light. At the end of the incubation, the cells were washed three times with 200 µL of PBS. Finally, the cells were counterstained with DAPI (diluted 1 : 1000 in PBS and incubated for 5 minutes at room temperature) and washed other three times with PBS. The cells were left in 200ul of PBS at 4 °C, protected from light before the acquisition with Leica STELLARIS 8 confocal microscope. Quantification of SCARA5 expression on acquired images were obtained by ImageJ software.

### Cell irradiation

$4.75 \times 10^5$ AB22 cells were seeded in twelve T25 flasks. After 24 h, four flasks were incubated with 50 µM of free [o-COSAN]$^-$

and four flasks with 50 μM of Apo:[o-COSAN]-nanohybrid. The remaining four flasks were used as control. At the end of the 16 h incubation, cells were washed with PBS and their medium was renewed. Two of the four flasks incubated with [o-COSAN]⁻ or Apo:[o-COSAN]⁻ nanohybrid and two flasks containing non-treated control cells were irradiated in the thermal column of the TRIGA Mark II reactor at the University of Pavia (Italy) for 15′ at 30 kW reactor power. After the irradiation, the medium was removed, replaced with fresh medium, and all the flasks were placed in a humidified atmosphere (5% $CO_2$, 37 °C) until the following day.

**Clonogenic assay**

Twenty-four hours after the irradiation, cells were detached using 0.05% trypsin and 0.02% EDTA, and a trypan blue exclusion assay was performed to assess cell viability of each cell sample. Cell viability was reported as a percentage of alive cells in treated and/or irradiated samples compared to control non-irradiated cells. Then, 200 AB22 cells from each differently treated flask were seeded in 6 cm diameter culture dishes to perform the clonogenic assay. Cells were allowed to grow for 10 days from the neutron irradiation, with medium renewal every 2–3 days. After this period, the cells were washed with PBS, fixed in methanol for 25 minutes, and stained with a solution of 0.5% (w/v) Crystal Violet in 20% ethanol for 30 minutes. The excess of Crystal Violet was then carefully removed, and the dishes were rinsed with tap water. Finally, they were left to dry in normal air at room temperature, scanned and analysed by ImageJ software to calculate their surface area covered by colonies.

## Conclusions

We successfully developed the Apo:[o-COSAN]⁻ nanohybrid, an innovative Apoferritin-based drug delivery system with the potential to improve dual cancer therapy by synergistically integrating chemotherapy and Boron Neutron Capture Therapy (BNCT). A high Apo loading capacity was achieved through a highly efficient encapsulation strategy, which involves disassembling the protein nanostructure under acidic conditions (pH = 2) followed by its reassembly at physiological pH. Specifically, 110 ± 31 boron atoms, corresponding to 6.1 ± 1.7 [o-COSAN]⁻ molecules, were effectively encapsulated within the inner cavity of Apoferritin, demonstrating the protein remarkable cargo-loading capability. Using higher [o-COSAN]⁻ concentrations, the peculiar ability of this compound to form micelles or aggregates that interact with the protein peptide subunits prevented proper reassembly of Apoferritin at neutral pH following acidic treatment. MCF7 breast cancer cells and AB22 mesothelioma cells were subsequently loaded with either free [o-COSAN]⁻ or Apo:[o-COSAN]⁻. The latter were then subjected to thermal neutron irradiation, and the extent of irreversible cellular damage was evaluated using viability and clonogenic assays.

## Author contributions

## Data availability

The data supporting this article have been included as part of the ESI.†

## Conflicts of interest

There are no conflicts to declare.

## Acknowledgements

## References

1 T. G. W. Edwardson, H. Cui, N. Saleh, J. S. Wang, B. Colson and E. Y. Wu, *Chem. Rev.*, 2022, **122**, 9145–9197.

2 A. A. A. Aljabali, M. Rezigue, R. H. Alsharedeh, M. A. Obeid, V. Mishra, Á. Serrano-Aroca and M. M. Tambuwala, *Pharm. Nanotechnol.*, 2022, **10**, 257–267.

3 M. Xu, S. Wei, L. Duan, Y. Ji, X. Han, Q. Sun and L. Weng, *Nanoscale*, 2024, **16**, 11825.

4 D. Finazzi and P. Arosio, *Arch. Toxicol.*, 2014, **88**, 1787–1802.

5 V. Bitonto, D. Alberti, R. Ruiu, S. Aime, S. Geninatti Crich and J. C. Cutrin, *J. Controlled Release*, 2019, **319**, 300–310.

6 Protein Data Bank, DOI: **10.2210/pdb3f32/pdb**.

7 L. S. Vedula, G. Brannigan, N. J. Economou, J. Xi, M. A. Hall, R. Liu, M. J. Rossi, W. P. Dailey, K. C. Grasty, M. L. Klein, R. G. Eckenhoff and P. J. Loll, *J. Biol. Chem.*, 2009, **284**, 24176–24184.

8 Z. Heger, S. Skalickova, O. Zitka, V. Adam and R. Kizek, *Nanomedicine*, 2014, **9**, 2233–2245.

9 B. Zhang, G. Tang, J. He, X. Yan and K. Fan, *Adv. Drug Delivery Rev.*, 2021, **176**, 113892.

10 Z. Tu, P. Timashev, J. E. Chen and X. J. Liang, *Biomater. Sci.*, 2021, **1**, e12022.

11 M. R. Ruggiero, D. Alberti, V. Bitonto and S. Geninatti Crich, *Inorganics*, 2019, **7**, 33.

12 F. K. Kálmán, S. Geninatti Crich and S. Aime, *Angew. Chem., Int. Ed.*, 2010, **49**, 612–615.

13 W. Li, S. Li, M. Zhu, G. Xu, X. Man, Z. Zhang, H. Liang and F. Yang, *J. Med. Chem.*, 2024, **67**, 17243–17258.

14 L. Cosottini, A. Geri, V. Ghini, M. Mannelli, S. Zineddu, G. Di Paco, A. Giachetti, L. Massai, M. Severi, T. Gamberi, A. Rosato, P. Turano and L. Messori, *Angew. Chem., Int. Ed.*, 2024, **63**, e202410791.

15 G. Ferraro, A. Pratesi, D. Cirri, P. Imbimbo, D. M. Monti, L. Messori and A. Merlino, *Int. J. Mol. Sci.*, 2021, **22**, 1874.

16 L. N. Turino, M. R. Ruggiero, R. Stefanìa, J. C. Cutrin, S. Aime and S. Geninatti Crich, *Bioconjugate Chem.*, 2017, **28**, 1283–1290.

17 R. F. Barth and J. C. Grecula, *Appl. Radiat. Isot.*, 2020, **160**, 109029.

18 S. Shen, S. Wang, D. Zhou, X. Wu, M. Gao, J. Wu, Y. Yang, X. Pan and N. Wang, *Int. J. Radiat. Biol.*, 2024, **100**, 1126–1142.

19 M. A. Dymova, S. Y. Taskaev, V. A. Richter and E. V. Kuligina, *Cancer Commun.*, 2020, **40**, 406–421.

20 K. Nedunchezhian, N. Aswath, M. Thiruppathy and S. Thirugnanamurthy, *J. Clin. Diagn. Res.*, 2016, **10**, ZE01–ZE04.

21 W. Huang, Y. Yang and Y. Pan, *Nano Res.*, 2024, **17**, 7479–7492.

22 D. Alberti, A. Toppino, S. Geninatti Crich, C. Meraldi, C. Prandi, N. Protti, S. Bortolussi, S. Altieri, S. Aime and A. Deagostino, *Org. Biomol. Chem.*, 2014, **12**, 2457–2467.

23 S. Okada, K. Nishimura, Q. Ainaya, K. Shiraishi, S. A. Anufriev, I. B. Sivaev, Y. Sakurai, M. Suzuki, M. Yokoyama and H. Nakamura, *Mol. Pharm.*, 2023, **20**, 6311–6318.

24 R. F. Barth, N. Gupta and S. Kawabata, *Cancer Commun.*, 2024, **44**, 893–909.

25 X. Zhang, L. M. Rendina and M. Müllner, *ACS Polym. Au*, 2023, **4**, 7–33.

26 M. Laird, K. Matsumoto, Y. Higashi, A. Komatsu, A. Raitano, K. Morrison, M. Suzuki and F. Tamanoi, *Nanoscale Adv.*, 2023, **5**, 2537–2546.

27 H. Xu, J. Liu, R. Li, J. Lin, L. Gui, Y. Wang, Z. Jin, W. Xia, Y. Liu, S. Cheng and Z. Yuan, *Coord. Chem. Rev.*, 2024, **511**, 215795.

28 A. Muñoz-Juan, M. Nuez-Martínez, A. Laromaine and C. Viñas, *Chem. – Eur. J.*, 2024, **30**, e202302484.

29 F. Teixidor, R. Núñez and C. Viñas, *Molecules*, 2023, **28**, 4449.

30 I. Fuentes, T. García-Mendiola, S. Sato, M. Pita, H. Nakamura, E. Lorenzo, F. Teixidor, F. Marques and C. Viñas, *Chem. – Eur. J.*, 2018, **24**, 17239–17254.

31 Y. Chen, A. Barba-Bon, B. Grüner, M. Winterhalter, M. A. Aksoyoglu, S. Pangeni, M. Ashjari, K. Brix, G. Salluce, Y. Folgar-Cameán, J. Montenegro and W. M. Nau, *J. Am. Chem. Soc.*, 2023, **145**, 13089–13098.

32 M. B. Troadec, D. M. Ward and J. Kaplan, *Dev. Cell*, 2009, **16**, 3–4.

33 J. Huang, D. L. Zheng, F. S. Qin, N. Cheng, H. Chen, B. B. Wan, Y. P. Wang, H. S. Xiao and Z. G. Han, *J. Clin. Invest.*, 2010, **120**, 223–241.

34 D. Ulker, Y. E. Ersoy, Z. Gucin, M. Muslumanoglu and N. Buyru, *Gene*, 2018, **673**, 102–106.

35 F. A. Flockerzi, J. Hohneck, M. Saar, R. M. Bohle and P. R. Stahl, *Diagnostics*, 2023, **13**, 2211.

36 S. Geninatti Crich, M. Cadenazzi, S. Lanzardo, L. Conti, R. Ruiu, D. Alberti, F. Cavallo, J. C. Cutrin and S. Aime, *Nanoscale*, 2015, **7**, 6527–6533.

37 S. Dacic, *Mod. Pathol.*, 2022, **35**, 51–56.

38 A. Lanfranco, S. Rakhshan, D. Alberti, P. Renzi, A. Zarechian, N. Protti, S. Altieri, S. Geninatti Crich and A. Deagostino, *Eur. J. Med. Chem.*, 2024, **270**, 116334.

39 J. Sforzi, A. A. Lanfranco, R. Stefania, D. Alberti, V. Bitonto, S. Parisotto, P. Renzi, N. Protti, S. Altieri, A. Deagostino and S. Geninatti Crich, *Sci. Rep.*, 2023, **13**, 620.

40 D. Alberti, A. Deagostino, A. Toppino, N. Protti, S. Bortolussi, S. Altieri, S. Aime and S. Geninatti Crich, *J. Controlled Release*, 2018, **280**, 31–38.

41 M. Sasai, H. Nakamura, N. Sougawa, Y. Sakurai, M. Suzuki and C. M. Lee, *Anticancer Res.*, 2016, **36**, 907–911.

42 D. Alberti, A. Michelotti, A. Lanfranco, N. Protti, S. Altieri, A. Deagostino and S. Geninatti Crich, *Sci. Rep.*, 2020, **10**, 19274.

43 M. Suzuki, H. Tanaka, Y. Sakurai, G. Kashino, L. Yong, S. Masunaga, Y. Kinashi, T. Mitsumoto, S. Yajima, H. Tsutsui, T. Sato, A. Maruhashi and K. Ono, *Radiother. Oncol.*, 2009, **92**, 89–95.

44 M. Nuez-Martínez, C. I. G. Pinto, J. F. Guerreiro, F. Mendes, F. Marques, A. Muñoz-Juan, J. A. M. Xavier, A. Laromaine, V. Bitonto, N. Protti, S. Geninatti Crich, F. Teixidor and C. Viñas, *Cancers*, 2021, **13**, 6367.

45 R. N. Grimes, *Carboranes*, 3rd edn, Academic Press, 2016.

46 M. F. Hawthorne, D. C. Young, P. M. Garrett, D. A. Owen, S. G. Schwerin, F. N. Tebbe and P. A. Wegner, *J. Am. Chem. Soc.*, 1968, **90**, 862.

47 D. C. Malaspina, F. Teixidor, C. Viñas and J. Faraudo, *Phys. Chem. Chem. Phys.*, 2023, **25**(41), 27942–27948.

48 I. Fuentes, T. García-Mendiola, S. Sato, M. Pita, H. Nakamura, E. Lorenzo, F. Teixidor, F. Marques and C. Viñas, *Chem. – Eur. J.*, 2018, **24**, 17239.

49 J. Plešek, *Chem. Rev.*, 1992, **92**, 269–278.

50 M. Tarrés, C. Viñas, P. González-Cardoso, M. M. Hänninen, R. Sillanpää, V. Dordović, M. Uchman, F. Teixidor and P. Matejíček, *Chem. – Eur. J.*, 2014, **20**, 6786–6794.

51 P. Cígler, M. Kožíšek, P. Řezáčová, J. Brynda, Z. Otwinowski, J. Pokorná, J. Plešek, B. Grüner, L. Dolečková-Marešová, M. Máša, J. Sedláček, J. Bodem, H. Kräusslich, V. Král and J. Konvalinka, *Proc. Natl. Acad. Sci. U. S. A.*, 2005, **102**, 15394–15399.

52 E. Canetta, E. Paul, J. Forbes, K. Azzouni, C. Viñas and F. A. J. Harwood, *Sci. Rep.*, 2015, **5**, 7804.

53 I. Fuentes, T. García-Mendiola, S. Sato, M. Pita, H. Nakamura, E. Lorenzo, F. Teixidor, F. Marques and C. Viñas, *Chem. – Eur. J.*, 2018, **24**, 17239.

54 I. Fuentes, J. Pujols, C. Viñas, S. Ventura and F. Teixidor, *Chem. – Eur. J.*, 2019, **25**, 12820.

55 J. A. M. Xavier, I. Fuentes, M. Nuez-Martínez, C. Viñas and F. Teixidor, *J. Mater. Chem. B*, 2023, **11**, 8422–8432.

56 U. Del Monte, *Cell Cycle*, 2009, **8**, 505–506, DOI: **10.4161/cc.8.3.7608.**.

57 S. Lindberg, J. Regberg, J. Eriksson, H. Helmfors, A. Muñoz-Alarcón, A. Srimanee, R. A. Figuero, E. Hallberg, K. Ezzat and Ü. Langel, *J. Controlled Release*, 2015, **216**, 58–66.

58 D. S. Chandrashekar, S. K. Karthikeyan, P. K. Korla, H. Patel, A. R. Shovon, M. Athar, G. J. Netto, Z. S. Qin, S. Kumar, U. Manne, C. J. Creighton and S. Varambally, *Neoplasia*, 2022, **25**, 18–27.

59 D. S. Chandrashekar, B. Bashel, S. A. H. Balasubramanya, C. J. Creighton, I. P. Rodriguez, B. V. S. K. Chakravarthi and S. Varambally, *Neoplasia*, 2017, **19**, 649–658.

60 M. F. Hawthorne and T. D. Andrews, *Chem. Commun.*, 1965, 443–444.

61 A. Zaulet, F. Teixidor, P. Bauduin, O. Diat, P. Hirva, A. Ofori and C. Viñas, *J. Organomet. Chem.*, 2018, **865**, 214–225.

62 J. C. Cutrin, S. Geninatti Crich, D. Burghelea, W. Dastrù and S. Aime, *Mol. Pharmaceutics*, 2013, **10**, 2079–2085.